UDC 623.438
DOI: 10.37128/2520-6168-2025-3-6

EXPERIMENTAL STUDY OF THE AMPLITUDE OF OSCILLATIONS ELASTIC–DAMPER SYSTEM (KELVIN–VOIGT BODY)

Stepan BEREHULIAK, Postgraduate Student
Lviv Polytechnic National University

БЕРЕГУЛЯК Степан Тарасович, аспірант
Національний університет «Львівська політехніка»

The paper investigates the influence of stiffness and damping on the oscillations of a spring-damper system under a given load (sprung mass). The stiffness determines the mass of the sprung part of a vehicle structure. The use of a damper in a typical configuration between the sprung and unsprung masses may, in some cases, help to attenuate vibrations, while in others, it may amplify them.

The aim of the experimental study is to empirically substantiate the rational parameters of the spring-damper system under a non-harmonic excitation of the oscillatory system by a force impulse of a given amplitude.

A laboratory test rig and the results of a factorial planned experiment are presented. A second-order regression equation in natural parameters was obtained. The regression model was analyzed with two factors – the sprung mass and the damping coefficient – while the stiffness coefficient was kept constant at three levels. For a stiffness coefficient of 3088 H/m and an excitation force impulse of 500 H applied to mass m_2, the oscillation amplitude of the sprung mass of 100 kg with a damping coefficient of 300 H·s/m is 48 mm, and with a damping coefficient of 200 H·s/m – 47 mm. For a sprung mass of 50 kg and damping coefficient of 300 H·s/m, the oscillation amplitude of mass m_2 is 88.9 mm, and with a damping coefficient of 200 H·s/m – 76.9 mm. Similarly, for a stiffness coefficient of 2745 H/m and excitation force impulse of 500 H, the oscillation amplitude of the sprung mass of 100 kg with a damping coefficient of 300 H·s/m is 55 mm, and with 200 H·s/m – 47 mm. For a sprung mass of 50 kg and damping coefficient of 300 H·s/m, the oscillation amplitude of mass m_2 is 108 mm, and with 200 H·s/m – 85.9 mm.

With a decrease in the sprung mass, the oscillation amplitude increases. A decrease in the stiffness coefficient of the spring-damper system also results in an increase in the oscillatory impulse amplitude of the sprung mass. A reduction in the damping coefficient of the spring-damper system leads to a decrease in the oscillatory impulse amplitude of the sprung mass. This enables adaptive control of the sprung mass oscillations while maintaining the condition of a damped oscillatory response of the spring-damper system.

Key words: *oscillation amplitude, stiffness coefficient, damper, sprung mass, factorial experiment, design matrix, factor, regression equation.*

Eq. 8. Fig. 3. Table. 3. Ref. 10.

1. Problem formulation

The study of elastic–damper systems is currently in high demand in the context of vehicle development. The suspension systems of vehicles, regardless of the type of transport system or suspension design, contain both elastic and damping elements. Elasticity determines the mass of the sprung part of the vehicle structure. The use of a damper in the typical configuration between the sprung and unsprung masses helps to attenuate oscillations in some cases, while in others it may induce them.

The necessity to alter the operating mode of the elastic–damper system under different conditions requires an adaptive system, which leads to the development of active or semi-active systems–those that control either elasticity or damping, or a combination of both elasticity and damping.

This, in turn, necessitates experimental studies of the parameters of the elastic–damper system.

2. Analysis of recent research and publications

Cylindrical helical compression springs are widely used in elastic–damper systems and in mechanical systems as energy storage components. Among their wide range of applications, those that require knowledge of the transverse stiffness of the spring pose significant challenges. Examples of such applications include vibratory conveyors, railway bogies, and vibration dampers.

Article received 24.10.2025. Article accepted 08.12.2025. Article published 25.12.2025.

Analytical models are generally based on simplifications and may therefore be prone to errors. Differences have been observed between experimental results and those obtained using elementary relations for the static characteristics of cylindrical helical compression springs [1]. Moreover, the stiffness relationships for springs available in the literature are sufficiently accurate only for springs with at least five active coils [2]. The cited work presents the results of experimental studies on the axial compression of springs with two different end types (closed and ground ends, and closed but unground ends). The influence of the end coils on the natural frequencies of longitudinal vibrations was analyzed [3]. A modification of the traditional analytical model was proposed, in which the fixed boundary points at the ends of the active coils were replaced by torsional stiffness elements representing the end coils. Including the end coils in the calculations produced results closer to experimental data than those obtained from the traditional model [3]. The problem of transverse vibrations of cylindrical helical compression springs, which has significant practical importance, has been addressed in many studies.

Researchers have investigated the use of a damper and a spring for in-wheel motor suspension and the development of a dynamic vibration absorber system that can simultaneously improve ride comfort and reduce in-wheel motor vibration compared to a conventional suspension system [4, 5]. Xu et al. studied the damping properties of viscoelastic dampers made of different viscoelastic materials [6, 7]. Sato et al. [8] proposed a method for evaluating the practical application of viscoelastic dampers in wind vibration control by using equivalent sinusoidal waveforms to simulate long-duration random excitations in the along-wind and cross-wind directions. Lu et al. [9] investigated the constitutive relationship of viscoelastic materials, taking into account the friction effect of individual molecular chains with the surrounding environment at the microscale.

The dynamic characteristics and energy dissipation behavior of viscoelastic dampers exhibit nonlinear dependence on both the frequency and the amplitude of displacement loading.

3. The purpose of the article

The purpose of the experimental study is to empirically substantiate the rational parameters of the elastic–damper system under non-harmonic excitation of the oscillatory system by an impulse of force with a given amplitude and duration.

4. Results and discussion

The parallel connection of an elastic element and a damping element represents the classical configuration of a Kelvin–Voigt body. The structural diagram of the test stand is shown in Figure 1, and its general view is presented in Figure 2.

The elastic elements (1) (Figures 1 and 2) are connected in parallel with a pneumatic damper (2). The pneumatic damper is connected to a subsystem (3) that measures pressure and includes a bypass throttle with a variable orifice. The information from subsystem (3) is transmitted to the damping control and monitoring system (DCMS), then to an analog-to-digital converter (ADC), from which data are read by a personal computer (PC).

Information about the oscillations of the sprung mass m_1 (6) and the unsprung mass m_2 (5) is captured by sensors (4), converted by the ADC, and then read by the computer. Control of the DCMS (see Figure 2, item 3, assembly) is carried out from the computer via a digital-to-analog converter (DAC). All measurement and processing operations are performed by the computer.

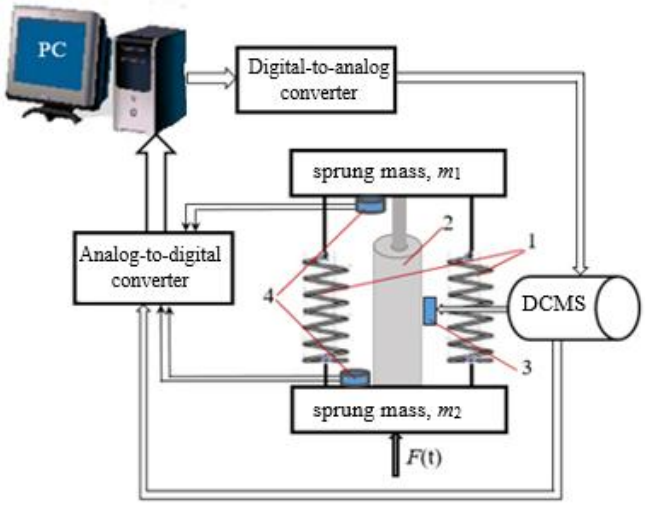

Fig. 1. Structural diagram of the test stand for investigating the elastic–damper system

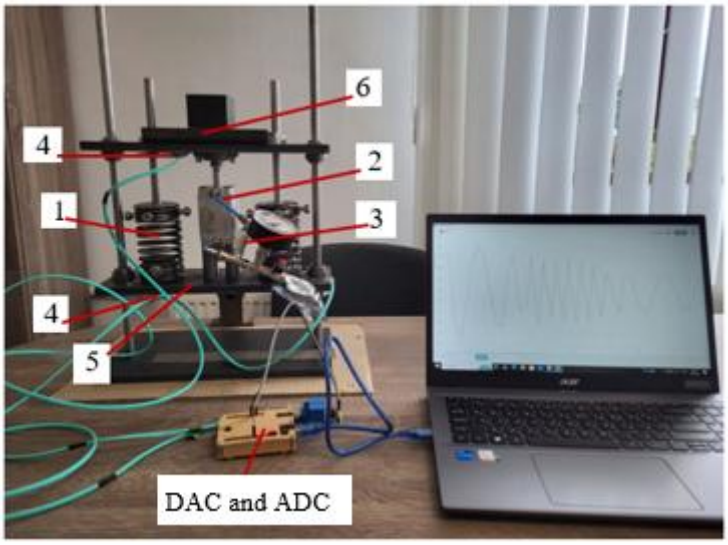

Fig. 2. General view of the test stand for investigating the elastic–damper system

The input factors include the sprung mass (m_1), the stiffness coefficient (K_{pr}), and the damping coefficient (K_{damp}). The response criteria are the oscillation amplitude of the sprung mass (A_{m1}) and the amplitude time constant (t_{puls}) of the sprung mass oscillation. The factor variation levels are given in Table 1. The study was conducted as a factorial designed experiment. The experimental methodology was based on the approach described in [10], taking into account the significance of each factor and decoding the regression model terms into coefficients corresponding to the natural values of the factors.

Table 1

Levels of variation of factors and their code values in the planned experiment

Factors	Designation	Dimension	Levels of factors			Variation interval
			upper	null	lower	
			Code values			
			+ 1	0	- 1	
Sprung mass, m_1	x_1	kg	100	75	50	25
Elasticity coefficient, K_{pr}	x_2	H/m	3088	2475	2402	343
Damping coefficient, K_{damp}	x_3	H·s/m	300	250	200	50

To investigate the influence of these factors, the experiment was carried out in three repetitions according to the experimental matrix (Table 2) and the previously described methodology [10].

In order for the design matrix to possess the property of orthogonality, a column with corrected level values x' was introduced in Table 2, which is calculated using the following formula:

$$\left(x_i'\right)^2 = x_i^2 - \frac{\sum x_i^2}{N}. \quad (1)$$

The matrix of calculated coefficients of the regression equation is presented in Table 2, where columns 2–11 constitute the orthogonal design matrix, column 12 – contain the experimental response values.

Based on the data from Table 2, the regression equation coefficients were calculated. The values of the regression coefficients characterize the contribution of each factor to the response function and were determined using the following formulas [10]:

$$b_1 = \frac{\sum(x_1 \cdot y)}{18}, \quad b_2 = \frac{\sum(x_2 \cdot y)}{18}, \quad b_3 = \frac{\sum(x_3 \cdot y)}{18}, \quad b_{11} = \frac{\sum((x_1')^2 \cdot y)}{6}, \quad b_{22} = \frac{\sum((x_2')^2 \cdot y)}{6}, \quad b_{33} = \frac{\sum((x_3')^2 \cdot y)}{6}, \quad b_{12} = \frac{\sum(x_1 \cdot x_2 \cdot y)}{12},$$

$$b_{13} = \frac{\sum(x_1 \cdot x_3 \cdot y)}{12}, \quad b_{23} = \frac{\sum(x_2 \cdot x_3 \cdot y)}{12}, \quad b_{123} = \frac{\sum(x_1 \cdot x_2 \cdot x_3 \cdot y)}{8},$$

$$b_0 = \frac{\sum y}{27} - 0.67 \cdot b_{11} - 0.67 \cdot b_{22} - 0.67 \cdot b_{33}. \quad (2)$$

The results of the coefficient calculations for the regression equation are presented in Table 3.

Table 2

Orthogonal Three-Factor Second-Order Design Matrix

№	x_1	x_2	x_3	$x_1 \cdot x_2$	$x_1 \cdot x_3$	$x_2 \cdot x_3$	$\left(x_1^{/}\right)^2$	$\left(x_2^{/}\right)^2$	$\left(x_3^{/}\right)^2$	$x_1 \cdot x_2 \cdot x_3$	y_1 (A_{m1}), m
1	2	3	4	5	6	7	8	9	10	11	12
1	+1	+1	+1	+1	+1	+1	0.3333	0.3333	0.3333	+1	0.0481
2	0	+1	+1	0	0	+1	-0.6667	0.3333	0.3333	0	0.06268
3	-1	+1	+1	-1	-1	+1	0.3333	0.3333	0.3333	-1	0.08895
4	+1	+1	-1	+1	-1	-1	0.3333	0.3333	0.3333	-1	0.0424
5	0	+1	-1	0	0	-1	-0.6667	0.3333	0.3333	0	0.0547
6	-1	+1	-1	-1	+1	-1	0.3333	0.3333	0.3333	+1	0.07688
7	+1	+1	0	+1	0	0	0.3333	0.3333	-0.6667	0	0.0429
8	0	+1	0	0	0	0	-0.6667	0.3333	-0.6667	0	0.05555
9	-1	+1	0	-1	0	0	0.3333	0.3333	-0.6667	0	0.07876
10	+1	-1	+1	-1	+1	-1	0.3333	0.3333	0.3333	-1	0.07338
11	0	-1	+1	0	0	-1	-0.6667	0.3333	0.3333	0	0.0962
12	-1	-1	+1	+1	-1	-1	0.3333	0.3333	0.3333	+1	0.13978
13	+1	-1	-1	-1	-1	+1	0.3333	0.3333	0.3333	+1	0.054
14	0	-1	-1	0	0	+1	-0.6667	0.3333	0.3333	0	0.06981
15	-1	-1	-1	+1	+1	+1	0.3333	0.3333	0.3333	-1	0.09865
16	+1	-1	0	-1	0	0	0.3333	0.3333	-0.6667	0	0.0588
17	0	-1	0	0	0	0	-0.6667	0.3333	-0.6667	0	0.07636
18	-1	-1	0	+1	0	0	0.3333	0.3333	-0.6667	0	0.1091
19	+1	0	+1	0	+1	0	0.3333	-0.6667	0.3333	0	0.0558
20	0	0	+1	0	0	0	-0.6667	-0.6667	0.3333	0	0.07567
21	-1	0	+1	0	-1	0	0.3333	-0.6667	0.3333	0	0.1088
22	+1	0	-1	0	-1	0	0.3333	-0.6667	0.3333	0	0.0473
23	0	0	-1	0	0	0	-0.6667	-0.6667	0.3333	0	0.0611
24	-1	0	-1	0	+1	0	0.3333	-0.6667	0.3333	0	0.08594
25	+1	0	0	0	0	0	0.3333	-0.6667	-0.6667	0	0.049
26	0	0	0	0	0	0	-0.6667	-0.6667	-0.6667	0	0.064
27	-1	0	0	0	0	0	0.3333	-0.6667	-0.6667	0	0.091
∑	18	18	18	12	12	12	-	-	-	8	-

To express the regression equation in natural factor values, the linear terms were transformed from coded values into natural values according to the formula [10]:

$$b_i x_i = \frac{b_i}{\varepsilon_i} X_i - \frac{b_i}{\varepsilon_i} X_{0i}, \quad (3)$$

where X_i – natural value of the factor, X_{i0} – natural value of the factor at the zero level, ε – variation interval.

The transformation of interaction linear terms was carried out according to the formula [10]:

$$b_{ij} x_i x_j = \frac{b_{ij}}{\varepsilon_i \varepsilon_j}\left(X_i X_j - X_i X_{0j} - X_j X_{0i} + X_{0i} X_{0j}\right). \quad (4)$$

The transformation of quadratic terms was performed using the formula [10]:

$$b_{ii} x_i^2 = \frac{b_{ii}}{\varepsilon_i^2}\left(X_i^2 - 2X_i X_{0i} + X_{0i} X_{0i}^2\right). \quad (5)$$

Analysis shows that the regression model with three factors would be inadequate. Therefore, the regression model is considered with two factors – the sprung mass and the damping coefficient – while the stiffness coefficient factor remains constant. Thus, for three values of the stiffness coefficient, we obtain three regression models.

The results of calculating the natural coefficients of the regression equation are given in Table 3.

Table 3

Results of the calculation of the regression equation coefficients at given levels of factor x_2

Coefficient of the regression equation	x_2 = +1		x_2 = 0		x_2 = -1	
	Coded coefficient	Real coefficient	Coded coefficient	Real coefficient	Coded coefficient	Real coefficient
b0	0.0555	0.1941	0.064	0.2033	0.076	0.257
b1	-0.0185	-0.001716	-0.0223	-0.001636	-0.0269	-0.001964
b2	0.0043	-0.000458	0.0077	-0.00051	0.0145	-0.000826
b12	-0.0016	$-1.28\cdot10^{-6}$	-0.0036	$2.88\cdot10^{-6}$	-0.0054	$-4.32\cdot10^{-6}$
b11	0.0054	$8.64\cdot10^{-6}$	0.0061	$9.76\cdot10^{-6}$	0.0082	$13.12\cdot10^{-6}$
b22	0.0032	$1.28\cdot10^{-6}$	0.0044	$1.76\cdot10^{-6}$	0.0072	$2.88\cdot10^{-6}$

The regression equations in natural parameters for the vibration of the sprung mass are as follows:

$$A_{m1(x2=+1)} = 0.1941 - 0.001716 \cdot m_1 - 0.000458 \cdot K_{damp} + \\ +8.64 \cdot 10^{-6} \cdot m_1^2 + 1.28 \cdot 10^{-6} \cdot K_{damp}^2 - 1.28 \cdot 10^{-6} \cdot m_1 \cdot K_{damp} \quad (6)$$

$$A_{m1(x2=0)} = 0.2033 - 0.001636 \cdot m_1 - 0.00051 \cdot K_{damp} + \\ +9.76 \cdot 10^{-6} \cdot m_1^2 + 1.76 \cdot 10^{-6} \cdot K_{damp}^2 + 1.76 \cdot 10^{-6} \cdot m_1 \cdot K_{damp} \quad (7)$$

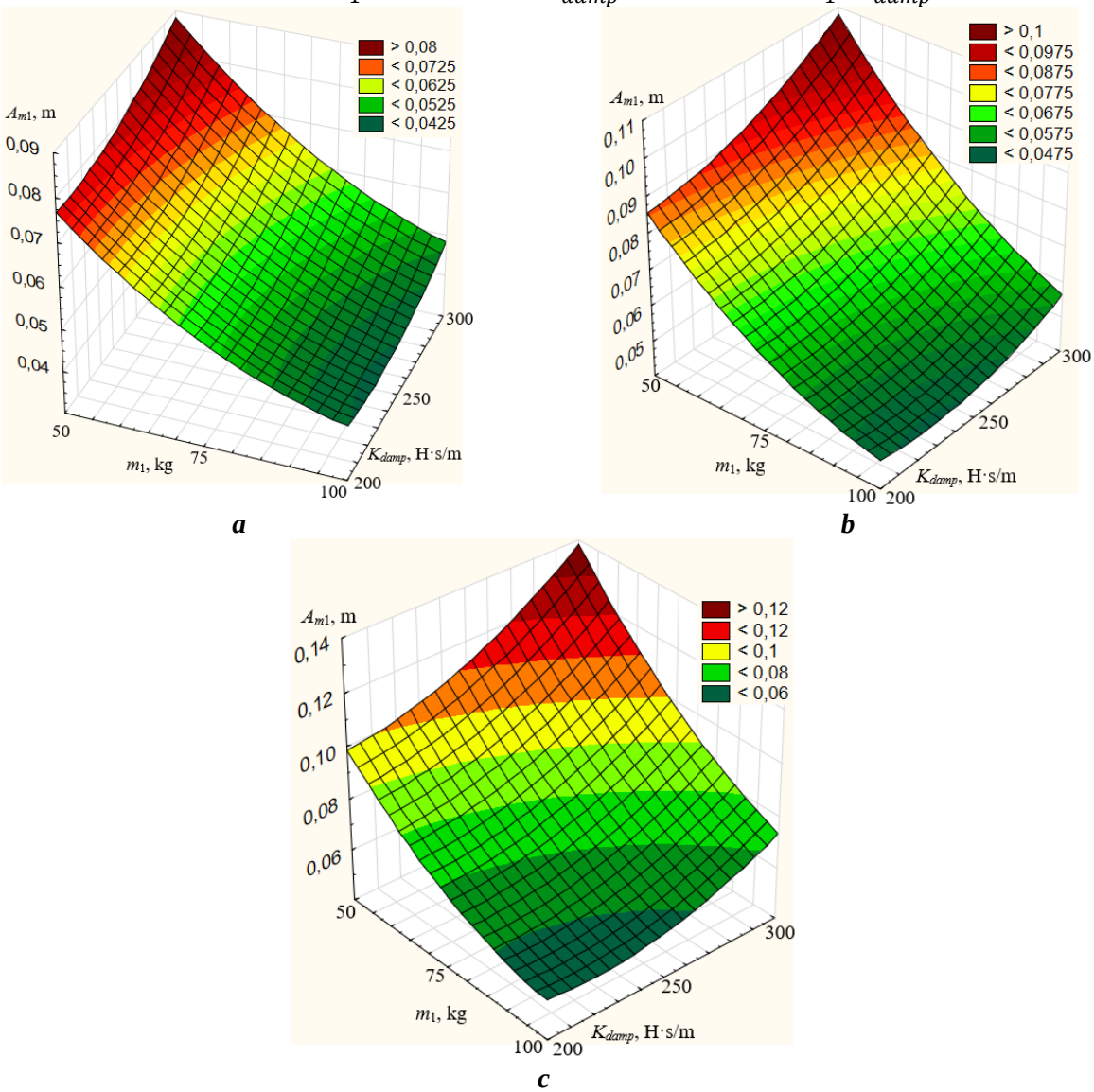

Fig. 3. 3D graphical models of the vibration amplitude of the spring-damper system as a function of the sprung mass m_1 and the damping coefficient K_{damp} at a given stiffness coefficient K_{pr} (H/m): a) 3088; b) 2475; c) 2402

$$A_{m1(x2=-1)} = 0{,}257 - 0.001964 \cdot m_1 - 0.000826 \cdot K_{damp} + \\ +13.12 \cdot 10^{-6} \cdot m_1^2 + 2.88 \cdot 10^{-6} \cdot K_{demp}^2 - 4.32 \cdot 10^{-6} \cdot m_1 \cdot K_{damp} \quad (8)$$

For a stiffness coefficient K_{pr} = 3088 H/m and an excitation impulse force $F(t)$ = 500 H applied to mass m_2 (Fig. 1), the amplitude of a single oscillation of the sprung mass m_1 = 100 kg is 48 mm at a damping coefficient K_{damp} = 300 H·s/m and 47 mm at K_{damp} = 200 H·s/m. With a decrease of the sprung mass, the oscillation amplitude increases (Eq. (6), Fig. 3a). For a sprung mass of 50 kg and K_{damp} = 300 H·s/m, the amplitude of a single oscillation of mass m_2 is 88.9 mm, while for K_{damp} = 200 H·s/m it is 76.9 mm. A decrease in the damping coefficient results in a reduction of the oscillation amplitude (Fig. 3a).

For a stiffness coefficient K_{pr} = 2745 H/m and the excitation impulse $F(t)$ = 500 H applied to mass m_2 (Fig. 1), the amplitude of a single oscillation of the sprung mass m_1 = 100 kg is 55 mm at K_{damp} = 300 H·s/m and 47 mm at K_{damp} = 200 H·s/m (Eq. (7), Fig. 3b). For a sprung mass of 50 kg and K_{damp} = 300 H·s/m, the amplitude of a single oscillation of mass m_2 is 108 mm, while for K_{damp} = 200 H·s/m it is 85.9 mm. A decrease in the damping coefficient leads to a reduction of the oscillation amplitude (Fig. 3b).

A similar trend of change in the amplitude of the oscillatory impulse is observed for the sprung mass m_1 = 75 kg. For K_{pr} = 2402 H/m, the trend of amplitude variation over the considered range of sprung masses is analogous (Eq. (8), Fig. 3c).

5. Conclusion

The analysis of the experimental data shows that with a decrease in the sprung mass (load mass), the amplitude of the oscillatory impulse of the sprung mass increases. A decrease in the stiffness coefficient of the spring-damper system also results in an increase in the oscillatory impulse amplitude of the sprung mass.

A reduction in the damping coefficient of the spring-damper system leads to a decrease in the oscillatory impulse amplitude of the sprung mass. This enables adaptive control of the sprung mass oscillations while maintaining the condition of a damped oscillatory response of the spring-damper system.

References

1. Yıldırım, V. (2016). Exact determination of the global tip deflection of both close-coiled and open-coiled cylindrical helical compression springs having arbitrary doubly-symmetric cross-sections. *International Journal of Mechanical Sciences, 115–116,* 280–298. DOI: https://doi.org/10.1016/j.ijmecsci.2016.06.022 [in English].
2. Paredes, M. (2016). Enhanced formulae for determining both free length and rate of cylindrical compression springs. *Journal of Mechanical Design, 138*(2), 021404. DOI: https://doi.org/10.1115/1.4032094 [in English].
3. Liu, H., & Kim, D. (2009). Effects of end coils on the natural frequency of automotive engine valve springs. *International Journal of Automotive Technology, 10*(4), 413–420. DOI: https://doi.org/10.1007/s12239-009-0047-8 [in English].
4. Liu, M., Gu, F., & Zhang, Y. (2017). Ride comfort optimization of in-wheel-motor electric vehicles with in-wheel vibration absorbers. *Energies, 10*(10), 1647. DOI: https://doi.org/10.3390/en10101647 [in English].
5. Qin, Y., He, C., Ding, P., et al. (2018). Suspension hybrid control for in-wheel motor driven electric vehicle with dynamic vibration absorbing structures. *IFAC-PapersOnLine, 51*(31), 973–978. DOI: https://doi.org/10.1016/j.ifacol.2018.10.054 [in English].
6. Xu, Z. D., Xu, C., & Hu, J. (2015). Equivalent fractional Kelvin model and experimental study on viscoelastic damper. *Journal of Vibration and Control, 21*, 2536–2552. DOI: https://doi.org/10.1177/1077546313513604 [in English].
7. Xu, Z. D., Liao, Y. X., Ge, T., & Xu, C. (2016). Experimental and theoretical study on viscoelastic dampers with different matrix rubbers. *Journal of Engineering Mechanics, 142*, 04016051. DOI: https://doi.org/10.1061/(ASCE)EM.1943-7889.0001101 [in English].
8. Sato, D., Osabel, D. M., & Kasai, K. (2022). Evaluation method for practical application of viscoelastic damper using equivalent sinusoidal waveforms of long-duration random excitations in along- and across-wind directions. *Engineering Structures, 254*, 113735. DOI: https://doi.org/10.1016/j.engstruct.2021.113735 [in English].
9. Lu, D., Xue, B., Cao, Y., & Chen, B. (2022). Constitutive theory for direct coupling of molecular frictions and the viscoelasticity of soft materials. *Journal of Applied Mechanics, 89*, 051007. DOI: https://doi.org/10.1115/1.4053728 [in English].

10. Dmytriv, V. T., Dmytriv, I. V., & Yatsunskyi, P. P. (2019). Experimental pulse generator combined with the milking machine collector. *INMATEH – Agricultural Engineering, 59*(3), 219–226. DOI: https://doi.org/10.35633/INMATEH-59-24 [in English].

ЕКСПЕРИМЕНТАЛЬНІ ДОСЛІДЖЕННЯ АМПЛІТУДИ КОЛИВАННЯ ПРУЖНО-ДЕМПФЕРНОЇ СИСТЕМИ (ТІЛО КЕЛЬВІНА-ФОЙГТА)

В роботі розглянуто вплив пружності і демпфування на коливання пружно-демпферної системи за заданого навантаження (підпружиненої маси). Пружність регламентує масу підпружиненої частини конструкції транспортного засобу. Використання демпфера в типовій конфігурації між підресореними та непідресореними масами в одних ситуаціях допомагає гасити коливання, а в інших – викликає їх.

Метою експериментального дослідження є емпіричне обґрунтування раціональних параметрів пружно-демпферної системи за негармонійного впливу на коливну систему імпульсу сили заданої амплітуди.

Приведено лабораторну установку та результати факторного планованого експерименту. Отримано рівняння регресії другого порядку в натуральних показниках. Регресійну модель розглядали за двома факторами, підружиненої маси і коефіцієнту демпфування, а фактор коефіцієнта пружності приймали незмінним на трьох рівнях. Для коефіцієнті пружності 3088 Н/m і силі імпульсу збурення 500 Н, яка прикладається до маси m_2, амплітуда коливання підпружинемої маси 100 kg за коефіцієнту демпфування 300 Н·s/m становить 48 mm, а за коефіцієнту демпфування 200 Н·s/m становить 47 mm. За підпружиненої маси 50 kg і коефіцієнті демпфування 300 Н·s/m амплітуда коливання маси m_2 становить 88,9 mm, а за коефіцієнту демпфування 200 Н·s/m, амплітуда одного коливання маси m_2 становить 76,9 mm. Аналогічно, за коефіцієнта пружності 2745 Н/m і силі імпульсу збурення 500 Н, амплітуда коливання підпружиненої маси 100 kg за коефіцієнту демпфування 300 Н·s/m становить 55 mm, а за коефіцієнту демпфування 200 Н·s/m становить 47 mm. За підпруженої маси 50 kg і коефіцієнті демпфування 300 Н·s/m амплітуда одного коливання маси m_2 становить 108 mm, а за коефіцієнту демпфування 200 Н·s/m, амплітуда одного коливання маси m_2 становить 85,9 mm.

Із зменшенням підпружиненої маси амплітуда коливання зростає. Із зменшенням коефіцієнту пружності пружно-демпферної системи амплітуда коливного імпульсу підпружиненої маси також зростає. Зменшення коефіцієнта демпфування пружно-демпферної системи веде до зменшення амплітуда коливного імпульсу підпружиненої маси. Це уможливлює адаптивне керування коливанням підпружиненої маси при забезпеченні умови затухаючого коливання пружно-демпферної системи.

Ключові слова: *амплітуда коливання, коефіцієнт пружності, демпфер, маса підпружинена, планований експеримент, матриця планування, фактор, рівняння регресії.*

Ф. 8. Рис. 3. Табл. 3. Літ. 10.

INFORMATION ABOUT THE AUTHOR

Stepan BEREHULIAK – Postgraduate Student of Department of Desing Machine and Automotive Engineering, Lviv Polytechnic National University, (79013, 12 Stepan Bandera Str., Lviv, Ukraine, e-mail: Stepan.T.Berehuliak@lpnu.ua, https://orcid.org/0009-0005-6597-9752).

БЕРЕГУЛЯК Степан Тарасович – аспірант кафедри проєктування машин та автомобільного інжинірингу, Національний університет «Львівська політехніка», (79013, вул. Степана Бандери, 12, м. Львів, Україна, e-mail: Stepan.T.Berehuliak@lpnu.ua, https://orcid.org/0009-0005-6597-9752).